Helical Flows and Asymmetry of Blood Jet in Dilated Ascending Aorta with Normally Functioning Bicuspid Valve

FAGGIANO, E.; ANTIGA, L.; PUPPINI, G.; QUARTERONI, A.; LUCIANI G.B.; VERGARA, C.

Helical Flows and Asymmetry of Blood Jet in Dilated Ascending Aorta with Normally Functioning Bicuspid Valve [*]

E. Faggiano[1], L. Antiga[2], G. Puppini[3], A. Quarteroni[1,4], G.B. Luciani[5]
and C. Vergara[6]

April 13, 2012

[1] MOX– Modellistica e Calcolo Scientifico
Dipartimento di Matematica "F. Brioschi"
Politecnico di Milano, Milano, Italy
elena.faggiano@mail.polimi.it, alfio.quarteroni@polimi.it

[2] Orobix S.r.l., Bergamo, Italy
luca.antiga@orobix.com

[3] Divisione di Radiologia, University of Verona, Verona, Italy
giovanni.puppini@ospedaleuniverona.it

[4] SB MATHICSE CMCS,
EPFL de Lausanne, Lausanne, Switzerland.
alfio.quarteroni@epfl.ch

[5] Division of Cardiac Surgery, University of Verona, Verona, Italy
giovannibattista.luciani@univr.it

[6] Dipartimento di Ingegneria dellInformazione e Metodi Matematici,
Università di Bergamo, Bergamo, Italy
christian.vergara@unibg.it

Abstract

Bicuspid aortic valve (BAV) is associated with aortic dilatation and aneurysm. Several studies evidenced an eccentric systolic flow in ascending aorta associated to increased wall shear stresses (WSS) and the occurrence of an helical systolic flow. This study seeks to elucidate the connections between jet asymmetry and helical flow in patients with normally functioning BAV and dilated ascending aorta. We performed a computational parametric study by varying, for a patient-specific geometry, the valve area and the flow rate entering the aorta and drawing also a tricuspid valve (TAV). We considered also phase contrast magnetic resonance imaging of four BAV and TAV patients. Measurement of normalized flow asymmetry (NFA) index, systolic WSS and of a new index (positive helic fraction, PHF) quantifying the presence of a single helical flow, were performed. In our computation, BAV cases featured higher values of all indices with respect to TAV in both numerical and imaged-based results. Moreover, all indices increased with decreasing valve area and/or with increasing flow rate. This allows us to identify two groups for BAV: the former with valve/root area ratio $r = 0.29$ and systolic flow rate $F > 18\,l/min$, or for $r < 0.29$, featuring high indices values ($NFA > 0.45$ and $PHF > 0.8$), and the latter featuring intermediate values ($0.2 < NFA < 0.4$, $0.5 < PHF < 0.7$).

1 Introduction

Bicuspid aortic valve (BAV), the most common congenital heart disease, is related to an increased prevalence of ascending aortic dilatation and aneurysm in normally functioning valvular regime when compared to tricuspid aortic valve (TAV) [5, 11, 18]. Besides the dominant hypothesis postulating a genetic origin for these vascular complications, in recent years a complementary (rather than alternative) functional hypothesis has received increasing attention: it states that the abnormal haemodynamics observed in patients with BAV could predispose to an enlargement of the ascending aorta and, possibly, to aneurysm formation [10, 4].

In particular, it has been established that eccentric flow jets occur in the ascending aorta of normally functioning BAV patients, see Fig. 1. Several techniques reported so far this phenomenon, in particular phase-contrast magnetic resonance imaging (PC-MRI) [14, 20, 8] and computational methods [23, 22, 6]. This asymmetry was found to be strictly related to increased wall viscous stresses exerted by the blood on the lumen surface, as highlighted in [3, 13] by PC-MRI techniques, and in [23, 22] by computational models. Wall blood stresses are supposed to play an important role in vascular remodeling and in aneurysm formation. Indeed, an increased haemodynamic load placed on the proximal aorta could possibly result in progressive aortic dilatation [7].
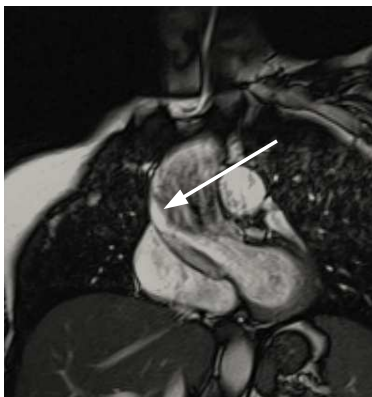
Figure 1: An oblique magnetic resonance image of an aortic arch in a BAV patient. Arrow indicates the blood flow deviation toward the aortic wall.

On the basis of these observations, the causes of formation and development of deflected flows has to be investigated in order to deeply understand the phenomenon of the dilatation of the ascending aorta in patients with normally functioning BAV. In this respect, an interesting observation is that blood flow jet asymmetry is also found in BAV patients featuring normal aortic dimensions [14]. This leads to formulating the conjecture that blood jet asymmetry may be due to the interplay between morphology and haemodynamics in BAV configurations and it precedes aorta dilatation. However, the latter seems to improve the jet deflection. Indeed, in [8], the authors found a significant correlation between the blood flow jet angle and the diameter at different levels of the ascending aorta.

Another phenomenon characterizing the abnormal fluid-dynamics in a BAV ascending aorta is the helical systolic flow [14]. In a normal TAV subject, retrograde/helical flows develop just at diastole, whilst in patients with ascending aortic aneurysm they originate at systole, together with a skewed peak velocity [15]. In patients with normally functioning BAV, systolic helical flow can appear in a normal ascending aorta, becoming particularly intense in dilated or aneurysmatic cases, as observed with PC-MRI in [14].

In this paper, we focus on the study of blood jet asymmetry in BAV patients with a dilated aorta but with non-stenotic aortic valve orifice. Our aim is to understand more deeply the phenomenon observed in [8]. In particular, we try to relate this phenomenon to the systolic helical flow observed with PC-MRI. With this goal, we consider the real geometry of a dilated BAV patient, and we perform a computational parametric study by varying the valve area (always in a non-stenotic range) and the flow rate entering the aorta. Besides we consider for the same dilated geometry a tricuspid valve in order to make comparisons with BAV cases. To find relations between haemodynamic phenomena, we introduce suitable indices, allowing us to monitor for each case the flow vorticity, the flow

reversal and the jet deflections. Finally, to further validate the correctness of the relation between helical flow and jet asymmetry found by our numerical results, we analyze PC-MRI images of BAV and TAV patients.

2   Material and Methods

2.1   Patient Dataset

A dataset was formed by four BAV patients without valve stenosis and insufficiency, and by four tricuspid (TAV) patients. In Table 1 several demographic information and aortic diameters for BAV patients (B) and TAV patients (T) are reported . Body surface area (BSA) was calculated by Haycock's formula [12] and was then used to normalize age and size effects in ascending aorta diameters calculation. All BAV patients had a dilated ascending aorta (ascending aorta diameter $\geq 4cm$ or normalized ascending aorta diameter $\geq 2.2cm/m^2$ [19]). Each BAV patient presented a right-left leaflets fusion.

Table 1: Demographic informations and aortic diameters for BAV (B) and TAV (T) patients.

	B1	B2	B3	B4	T1	T2	T3	T4
Age (y)	39	46	38	22	21	21	24	21
Sex (M,F)	F	M	M	M	F	M	M	F
BSA(m^2)	1.7	2.2	2.5	2.0	1.4	1.8	1.9	1.8
Anulus (cm)	2.5	2.0	3.2	3.5				
SV (cm)	3.4	2.7	4.8	3.6				
STJ (cm)	3.7	2.4	4.4	4.1				
AAo (cm)	4.0	5.0	5.0	4.1	2.5	3.1	2.7	2.6
AAo/BSA (cm/m^2)	2.4	2.3	2.0	2.0	1.8	1.7	1.4	1.4

B, Bicuspid aortic valve; T, tricuspid aortic valve; BSA, Body surface area; SV, sinus of valsalva; STJ, sinotubular junction; AAo, ascending aorta; AAo/BSA, normalized AAo size.

For each BAV and TAV patient a time-resolved 2D PC-MRI was acquired. An oblique imaging slice (PC-slice) was positioned in the mid-ascending aorta approximately at $2\,cm$ from the most distal feature of the sinotubular junction, as can be seen in Fig. 2. Temporal resolution was 20 phases in one cardiac cycle with a pixel resolution of 1.17×1.17 mm. Velocity encoding values were chosen to optimize the velocity map resolution with values ranging from 150 to 200 cm/s. The following parameters were also used: TE = 6.4 ms; flip angle $= 15\,\mathrm{deg}$; slice thickness = 5 mm;
acquisition matrix $= 256 \times 256$.

A breath-hold true fast imaging with steady state precession (TrueFisp) cine-
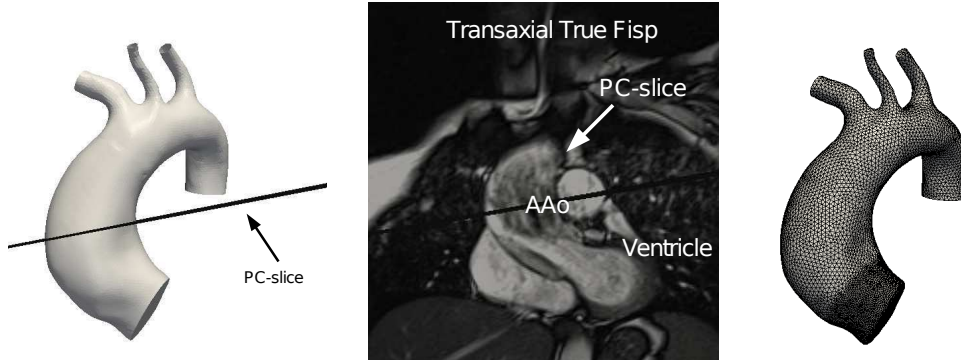
Figure 2: Aortic arch reconstruction for a selected BAV patient (left), and related oblique TrueFisp image (center). In both pictures the plane of acquisition of the PC-MRI image is depicted (PC-slice). On the right the solid model after the refinement step; the mesh was refined close to the valve.

sequence with retrogated ECG triggering was also acquired on oblique coronal slices, see Fig. 2, center. For a multiphase imaging of the bicuspid aortic valve, TrueFisp images were acquired also on the valve plane. Oblique and valve True-Fisp images were performed using to the following parameters: TE = 1.6 ms; flip angle = 65 deg ; slice thickness = 8 mm; temporal resolution = 20 phases in one cardiac cycle ; acquisition matrix = 256 × 146.

For BAV patients a 3D contrast enhanced MRI (CE-MRI) was acquired with a voxel resolution of 1.72 × 1.72 × 1.5 mm. The following parameters were used: TE = 1.02 ms; flip angle = 20 deg ; slice thickness = 1.5 mm; acquisition matrix = 256 × 106.

All the MRI acquisitions were performed on a 1.5 Tesla system (Magnetom Simphony, Siemens Medical Systems, Erlangen, Germany)

Institutional Review Board approval was obtained for the conduct of this study and the board waived the need for patient consent.

2.2 Mesh generation

A surface model of the aortic root, ascending aorta and aortic arch of one of the four BAV patients (B1) was obtained from the 3D CE-MRI image using a level-set segmentation technique provided by the Vascular Modeling Toolkit (vmtk, http://www.vmtk.org). This technique allows the generation of a surface representing the interface between the blood and the arterial wall. The surface was then cut at the aortic root inlet with a plane corresponding to the TrueFisp valve acquisition and at the outlets by planes perpendicular to the lumen longitudinal axis. We then manually delineated the valve orifice on the aortic root inlet surface, by using a tool which allows to choose the valve shape, dimension and position.

In this work we were interested in describing the systolic fluid-dynamics, so that we computed by the TrueFisp image the values of the valve and root areas, A_{val} and A_{root}, at systole. Since the CE-MRI acquisition could be assimilated to the diastolic phase of the cardiac cycle, we mapped the systolic valve orifice obtained by the TrueFisp image onto this diastolic configuration (Bn1), by maintaining the value A_{val}/A_{root} constant. Moreover, in view of the parametric study, we delineated two more different bicuspid valve orifices (Bn2 and Bn3) with a shape similar to the original one, always maintaining the valve area in a non-stenotic range. A tricuspid orifice (Tn) was also delineated to simulate in the same aorta geometry the tricuspid case. In Fig. 3 the TrueFisp image at systole and the four valve (Bn1, Bn2, Bn3 and Tn) are shown. In table 2 the values of A_{val}/A_{root} ratio and of A_{val} for patient B1 and for the four simulated cases are reported.
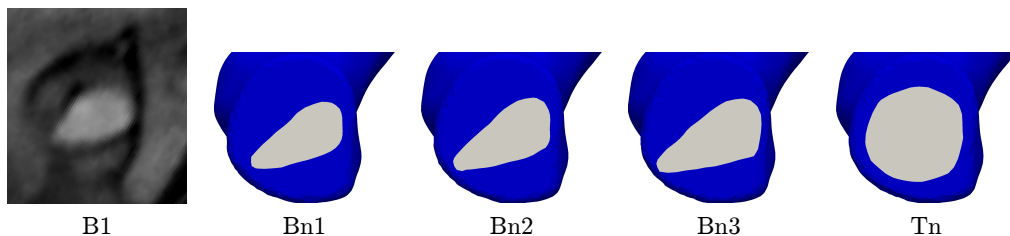

| B1 | Bn1 | Bn2 | Bn3 | Tn |

Figure 3: TrueFisp image of the aortic valve orifice of BAV patient 1 (B1) in the systolic phase (left) and the reconstructed valve orifices on the surface model of the same patient (Bn1, Bn2, Bn3 and Tn).

Table 2: Values of A_{val}/A_{root} and A_{val} for B1 patient (at systole, from True-Fisp image) and for the reconstructed valve orifices (mapped onto the diastolic configuration).

	B1	Bn1	Bn2	Bn3	Tn
A_{val}/A_{root}	0.26	0.26	0.29	0.33	0.51
A_{val} (mm^2)	2.5	1.6	1.8	2.0	3.1

The obtained solid models were successively turned into volumetric meshes of linear tetrahedra [1] using vmtk, in order for computational fluid-dynamics (CFD) simulations to be carried out (see Fig. 2, right). We observe the refined surface meshes in the area near the valve for better capturing the expected detachment and deviation of the flow. All the meshes featured about 600k tetrahedra.

2.3 Numerical Simulations

Unsteady numerical simulations were performed in the four scenarios described above, by using the finite element library LifeV (http://www.lifev.org). Blood

was considered as Newtonian, homogeneous, and incompressible, so that the Navier-Stokes equations for incompressible fluids were used for the mathematical description [9]. Blood viscosity was set equal to 0.035 Poise and the density equal to $1.0\,g/cm^3$. The time step was chosen equal to 0.01s. Being interested in the haemodynamics at systolic ejection, the vessel wall was considered rigid and valve leaflets were not modeled as assumed not influencing the direction of the jet at systole, due to the high pressure of blood exiting from the left ventricle. Valve opening and closing were therefore modeled in an on/off modality. We considered the patient specific shape measured by PC-MRI (Fig. 4), and we prescribed three different curves obtained by the original one multiplied by 1, 1.2 and 1.4 (F0, F2, F4), respectively, obtaining a flow rate at systole equal to 13.63, 16.36 and 19.09 l/min, respectively. The choice of prescribing flow
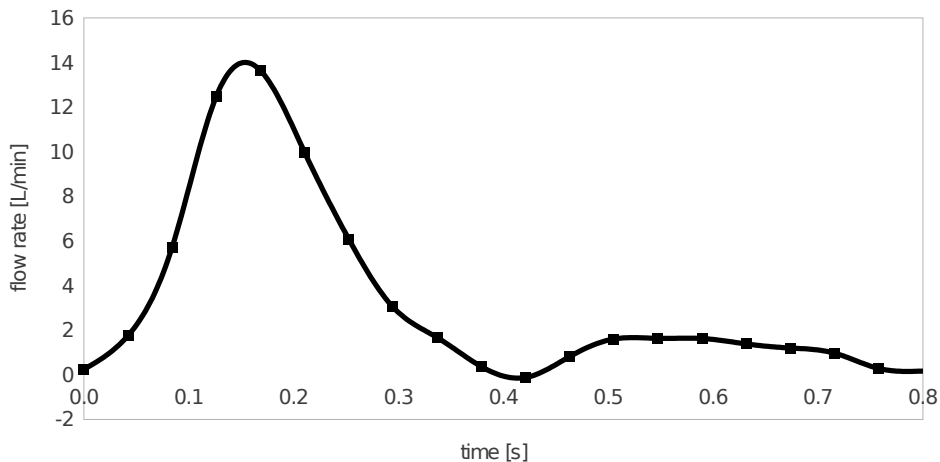

Figure 4: Flow rate curve obtained from PC-MRI images of patient B1.

rates greater than the measured one was suggested by the fact the PC-MRI often under-estimates the flux values [2]. To prescribe this flow rate a Lagrange multipliers' approach was employed [21]. At the outlets, a zero-stress condition was prescribed, since the region of interest is in the proximal ascending aorta. It must be highlighted that, as pointed out in [17], in TAV cases transitional flow are only expected to be present near the aortic valve, supposedly being absent in the ascending aorta. We assumed that this hypothesis holds also for BAV cases, so that no turbulence models were assumed.

2.4 Quantitative Measures

To better describe the fluid-dynamics in the ascending aorta we introduced suitable indices to be computed starting from both the results obtained in our numerical simulations and image data.

For the latter we processed the phase contrast images for each BAV and TAV case to obtain a velocity vector field. We point out that the following indices were defined on a triangular grid for the numerical results, while on a pixelized grid for the in-vivo data.

(a) *Retrograde flow analysis.* To quantify the retrograde flow we measured the flow reversal ratio (FRR) at systole at the PC-slice Γ, defined as

$$FRR = \frac{|Q_{neg}(t_{sys})|}{Q_{pos}(t_{sys})} \times 100,$$

where $Q_{neg}(t_{sys}) := \int_\Gamma \mathbf{v}^-(t_{sys}) \cdot \mathbf{n} \, d\sigma$ and $Q_{pos}(t_{sys}) := \int_\Gamma \mathbf{v}^+(t_{sys}) \cdot \mathbf{n} \, d\sigma$, with $\mathbf{v}^- \cdot \mathbf{n}|_\Gamma \leq 0$ and $\mathbf{v}^+ \cdot \mathbf{n}|_\Gamma > 0$, represent the backward and forward flow rates.

(b) *Flow asymmetry.* To quantify flow eccentricity we used the normalized flow asymmetry index (NFA) proposed in [20]. NFA was calculated as the euclidean distance between the center of velocity at Γ of the forward flow C_{vel} at systole, defined as

$$C_{vel,j} = \frac{\int_\Gamma j\mathbf{v}^+(t_{sys}) \cdot \mathbf{n} \, d\sigma}{\int_\Gamma \mathbf{v}^+(t_{sys}) \cdot \mathbf{n} \, d\sigma} \qquad j = x, y, z,$$

and the center of Γ normalized to the lumen radius. Lumen radius has been computed by mapping the lumen onto a circle. This yields a NFA index equal to 0 when the center of forward velocity is in the center of the vessel (no asymmetric flow) and equal to 1 when it is on the vessel wall (totally asymmetric flow).

(c) *Wall Shear Stress.* We introduced two wall shear stress indices, WSSRegion and WSSSlice which are the maximum of wall shear stress evaluated on a portion of the ascending aorta and on the PC slice, respectively [22].

(d) *Helical flow pattern analysis.* We introduced a new quantitative index to measure the helical flow pattern. We preliminarily defined the quantity h calculated over the PC slice as the dot product between the vorticity of the velocity parallel to the slice and the normal to the slice, $h := (\nabla \times (\mathbf{v}(\mathbf{t}) \cdot \boldsymbol{\tau})) \cdot \mathbf{n}$, where $\boldsymbol{\tau}$ is the tangential to the slice unit vector. h_i is then defined for each triangle (or pixel) of the slice and is positive or negative if the flow has a local right-handed or left-handed helical structure, respectively. The positive helic fraction (PHF) at systole was then calculated as

$$PHF = \frac{H_{pos}}{H_{pos} + H_{neg}},$$

where $H_{pos} = \int_\Gamma h^+(t_{sys}) \, d\sigma$ and $H_{neg} = \int_\Gamma h^-(t_{sys}) \, d\sigma$, with $h^+ > 0$ and $h^- < 0$. PHF indicates the ratio between right-handed helic and the totality of the rotating flux (PHF=1 means complete right-handed helical flow,

8

PHF=0 means complete left-handed helical flow, PHF=0.5 means no prevalence of any direction), and was introduced to quantify the prevalence of right-handed helical flow in BAV patients. To eliminate border effects due to no-slip data we cut with a sphere the PC-slice and calculated the PHF index only inside the extracted area.

For the computation of such indices we developed a tool based on the the Visualization Toolkit library (VTK, http://www.vtk.org).

The integrals in the formulas were calculated using mean point quadrature rule.

3   Results

This section is divided in two parts. In the first part we report the results of the CFD simulations for the different valve orifices described in Section 2.2 and the different inflow boundary conditions described in Section 2.3. After a first view of the overall flow pattern in the ascending aorta, we present the values obtained for the proposed indices. In the second part we analyze the in-vivo data computing the same indices to confirm and strengthen the numerical findings.

3.1   Numerical Simulations

3.1.1   Preliminary analysis

A first snapshot of the flow pattern in the ascending aorta is shown in Fig. 5. In this figure the streamlines entering the PC-slice at systole are reported for three significative cases: the largest bicuspid valve with the lowest inflow condition (Bn3, F0), the smallest bicuspid valve with the highest inflow condition (Bn1, F4) and the tricuspid case with the mid-value inflow condition (Tn, F2). From this figure the marked difference between the fluid-dynamics in the first tract of the ascending aorta in TAV and BAV cases could be appreciated. Indeed, in the BAV cases we observed a single recirculating vortex that forces the flow exiting from the valve to deviate toward the aortic wall. From a comparison between the two BAV cases, we preliminary observed that the more the valve is narrowed and/or the flow rate is high, the more the vortex is enlarged, making the deviation of the jet more evident (see Fig. 5, left and middle). Concerning the TAV case, we observed recirculation zones characterized by a double vortex, whose formation is justified by the dilated geometry of the chosen aorta (see [15]). Also the location of the vortices is different, since in the TAV case one vortex was located just in the zone where the jet hit the wall in the BAV cases. No deviation of the flow exiting the valve could be appreciated in TAV case (Fig. 5, right).
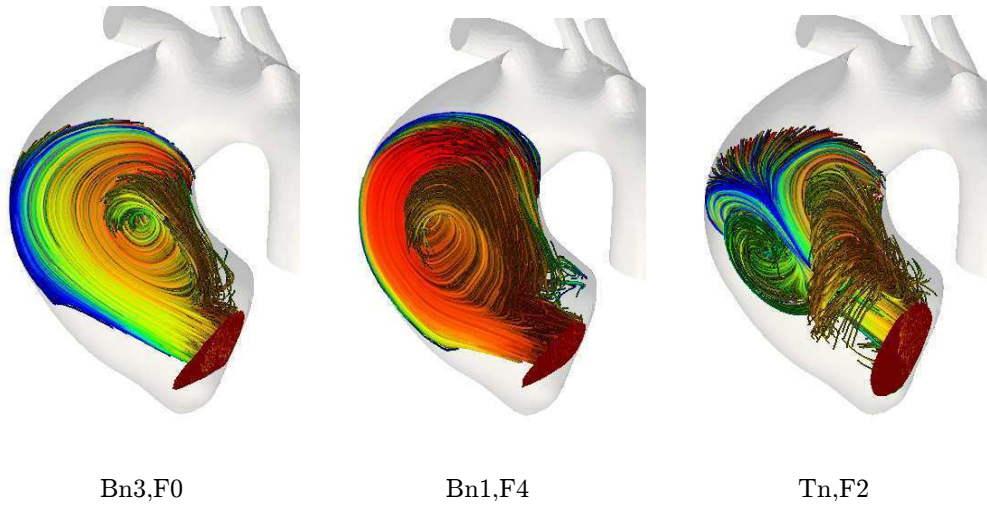
| Bn3,F0 | Bn1,F4 | Tn,F2 |

Figure 5: Streamlines of the velocity fields in three significant cases.

3.1.2 Retrograde flow analysis

All the simulated BAV presented a retrograde flow at systole at the PC-slice. In Table 3 the values of FRR for all the simulations are reported. We observe that, except the case Bn2-F0, FRR increases by decreasing the area of the orifice or by increasing the flow rate. In all tricuspid cases FRR is very small (more than 100 times smaller than Bn3) indicating no retrograde flow for this configuration. For the BAV cases this index features higher values, reaching almost the value of 30%.

Table 3: FRR index (in %) for numerical simulations.

Valve/Flux	F0	F2	F4
Bn1	13.46	24.81	29.91
Bn2	14.77	14.14	19.27
Bn3	1.31	8.82	17.64
Tn	0.0	0.06	0.07

3.1.3 Flow asymmetry

All simulated BAV presented an evident deviation of the flow toward the aortic wall, which was completely absent in the tricuspid case. In Fig. 6 we reported on an oblique TrueFisp slice the velocity pattern at systole obtained by numerical results in a BAV (middle) and in a TAV case (right). In the BAV case the flow originates straight from the valve and it then deviates toward the outer wall. A completely different situation occurs for TAV, where the flux does not

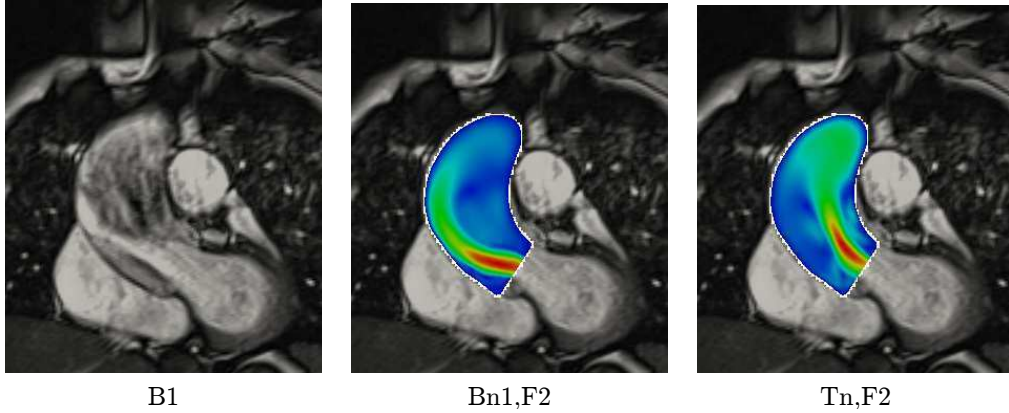|		
B1	Bn1,F2	Tn,F2

Figure 6: Velocity patterns obtained by the numerical solutions reported on the oblique TrueFisp slice on the left.

deviate toward the wall but goes straight covering the shortest path to reach the mid-ascending aorta.

In Table 4 the values of the NFA index are reported for all the cases. This in-

Table 4: NFA index for numerical simulations.

Valve/Flux	F0	F2	F4
Bn1	0.46	0.51	0.48
Bn2	0.31	0.37	0.47
Bn3	0.24	0.36	0.36
Tn	0.08	0.14	0.14

dex features a behavior similar to that of FRR. Indeed, it seemed to be inversely proportional to the valve orifice dimension and directly proportional to the flow rate. In tricuspid cases, as expected, the NFA value was smaller, indicating an almost total absence of flow deviation. We could subdivide the cases in three subpopulations: marked flow asymmetry (NFA≥ 0.46; Bn1 and Bn2-F4), moderate flow asymmetry ($0.24 < $ NFA $ < 0.38$; Bn2-F0, Bn2-F2 and Bn3) and no flow asymmetry (NFA $ < 0.15$; Tn).

3.1.4 Wall Shear Stress

In Fig. 7 left, we reported the regions of interest where the quantities WSSRegion and WSSSlice were computed, whereas, in Table 5 and 6 WSSRegion and WSSSlice are reported for all the performed simulations.

As expected WSS values were low in the tricuspid case and in the simulation with Bn3-F0, which is the case with larger valve area and lower flow. When decreasing the valve area and increasing fluxes, the WSS values become higher up to 3 times the values obtained for the higher tricuspid case.
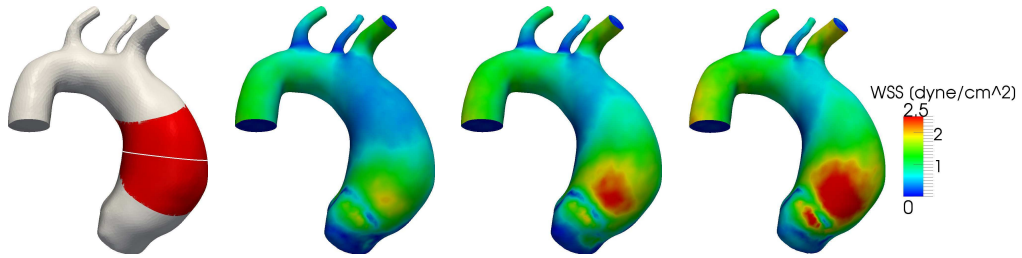
Figure 7: Left: in red the area in which WSSRegion was measured and in white the line along which WSSSlice was measured. Next: WSS values for Bn1-F0, Bn1-F2 and Bn1-F4.

Table 5: Values of index WSSRegion for the numerical simulations ($dyne/cm^2$).

Valve / Flux	F0	F2	F4
Bn1	1.95	2.61	3.34
Bn2	0.97	1.25	1.77
Bn3	0.85	1.11	1.19
Tn	0.48	0.78	0.96

Table 6: Values of index WSSSlice for the numerical simulations ($dyne/cm^2$).

Valve / Flux	F0	F2	F4
Bn1	0.85	1.60	1.85
Bn2	0.70	1.11	1.76
Bn3	0.46	0.71	0.91
Tn	0.28	0.48	0.59

Finally, as shown in Fig. 7, the higher WSS values were found to be located for BAV cases in the typical location of aortic dilatation.

3.1.5 Helical flow pattern analysis

In Fig. 8 a top view of the PC-slice with the computed velocities in all the simulated cases are shown. It is evident from this figure the presence of a right-handed helical flow in BAV cases which is completely absent in TAV. At the bottom of each case, the quantity h is depicted in a color scale (red colors stand for $h > 0$, i.e. local right-handed helical structure, blue colors stand for $h < 0$, i.e. local left-handed helical structure and green colors stand for $h = 0$, i.e. no local helical structure). In Table 7 we reported the values of index PHF for all the simulated cases. We observe that this index succeeded in describing the phenomenon highlighted by Fig. 8. Indeed, if we consider for example Bn1-F2, the high prevalence of the right-handed helic is captured (PHF = 0.89), while Tn-F2, for example, did not present a prevalence of one helic over the other
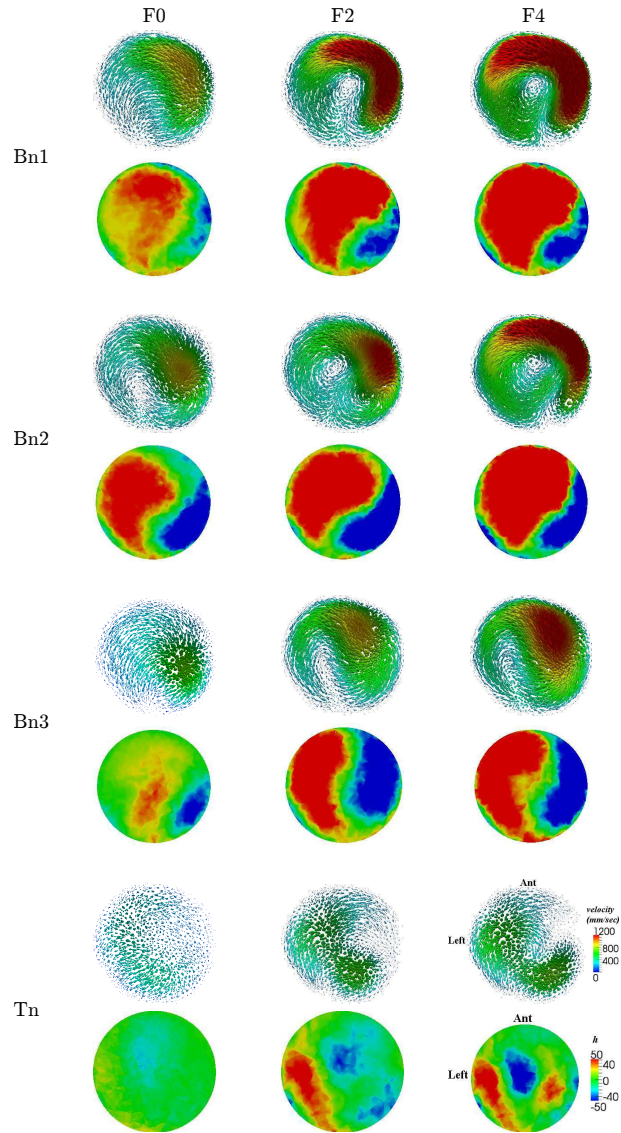
Figure 8: Top view of the PC-slice with the computed velocities and the corresponding h values for all the simulations. h red colors stand for $h > 0$, i.e. local right-handed helical structure, blue colors stand for $h < 0$, i.e. local left-handed helical structure and green colors stand for $h = 0$, i.e. no local helical structure.

(PHF=0.45).

More in general, all BAV cases were characterized by a right-handed helical flow, which become more pronounced with smaller valve areas and higher flows (for BAV cases, PHF values ranges from 0.60 to 0.89). We could collect the cases depending on the value of the PHF index in the same three groups introduced above for the flow asymmetry: high right-handed prevalence (PHF$\geq$ 0.8; Bn1

13

and Bn2-F4), low right-handed prevalence ($0.6 <$ PHF < 0.7; Bn2-F0, Bn2-F2 and Bn3) and no right-handed prevalence (PHF < 0.5; Tn).

Table 7: Values of index PHF for numerical simulations.

Valve / Flux	F0	F2	F4
Bn1	0.85	0.89	0.90
Bn2	0.61	0.61	0.83
Bn3	0.69	0.60	0.64
Tn	0.23	0.45	0.47

3.2 Data from biomedical images

The proposed indices calculated on clinical data are reported in Table 8. These

Table 8: Systolic flow rate and ratio between the valve and root areas (top) and proposed indices (bottom) evaluated in BAV (B) and TAV (T). Average Values for BAV (Avg B) and TAV (Avg T) are also reported.

	B1	B2	B3	B4	T1	T2	T3	T4	Avg B	Avg T
Q_{sys}	13.63	7.93	21.60	6.51	21.38	24.35	31.86	32.35		
A_{val}/A_{root}	0.26	0.25	0.27	0.51						
FRR	46.72	55.77	49.66	43.78	0.98	3.59	1.81	0.20	48.98	1.65
NFA	0.59	0.61	0.61	0.23	0.01	0.06	0.07	0.02	0.51	0.04
PHF	0.82	0.55	0.83	0.55	0.22	0.23	0.16	0.06	0.69	0.24

data confirmed the presence of a retrograde flow, flow jet asymmetry and helic systolic flow in all BAV cases, being absent in the four TAV patients. Indeed, the average value of the three indices (see right column) was clearly larger in BAV patients. Despite the small number of subjects included in the study, in Table 8 we could recognize the same trends featured by our numerical simulations. Three of the four BAV patients had a similar A_{val}/A_{root} ratio (B1, B2 and B3, A_{val}/A_{root} equal to 0.26, 0.27 and 0.25, respectively). These three patients, as expected, presented similar values of FRR, NFA and PHF indices, except PHF value for B2 which is lower. A possible explanation is that this case featured a systolic flow rate of $7.9\,l/min$, considerably lower than those of the two other patients with similar valve orifices. B4 had a greater valve orifice (A_{val}/A_{root}=0.51) and, as expected, presented values of the three indices lower than for the other patients. The trend highlighted by PHF is confirmed also by the visual inspection of the velocity field and of the quantity h reported in Fig. 9. In patients with small valve orifice (B1,B2 and B3) the red zone, representing right-handed helical flow, is more pronounced with respect to the blue (left-handed helical flow) and to the green (absence of helical flow) zones.

For what concerns TAV cases, Table 8 highlights that the values of all the three indices are significantly smaller than those featured by BAV patients, confirming the trend observed by numerical simulations. Fig. 9 confirms the absence
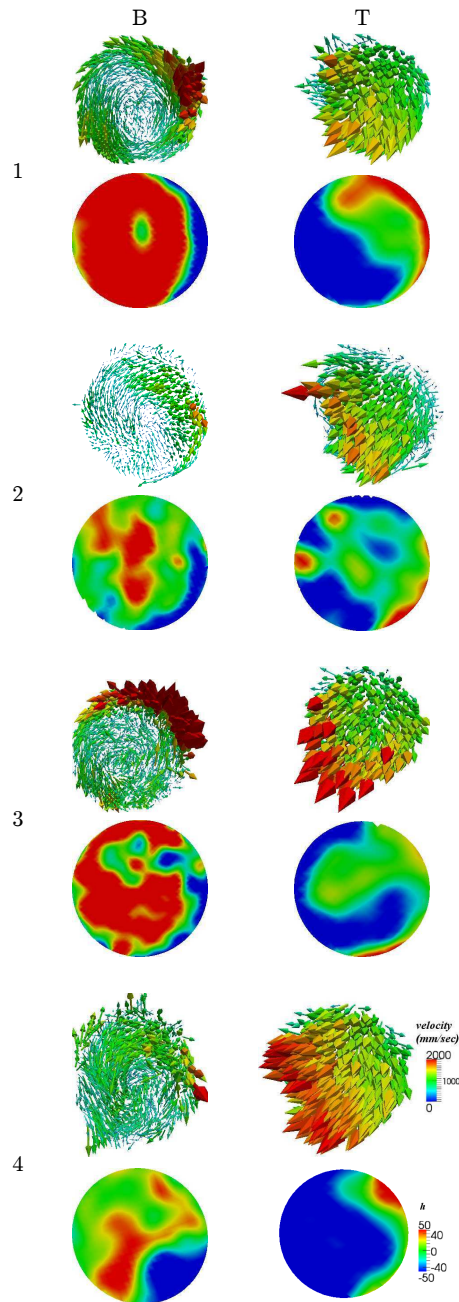
Figure 9: Top view of the PC-slice with the measured velocities and the corresponding h values for all the patients and controls. h red colors stand for $h > 0$, i.e. local right-handed helical structure, blue colors stand for $h < 0$, i.e. local left-handed helical structure and green colors stand for $h = 0$, i.e. no local helical structure

15

of a right-handed helical flow in these cases, featuring mainly blue and/or green zones.

4   Discussion

In recent years considerable attention was devoted to the study of the "haemodynamic hypothesis", stating that the strong connection observed between BAV patients and the formation of ascending aortic dilatation could be provided, besides genetic factors, also by haemodynamic factors. In particular, this hypothesis states that the deranged flow which is found in BAV patients could cause enlargement of the ascending aorta and, possibly, aneurysm formation [5, 10, 4, 18]. The first characteristic fluid-dynamic phenomenon featured by BAV patients reported by several studies, both in-vivo and in-silico, consists in the presence of an eccentric flow jet in the ascending aorta [14, 20, 23, 22, 6, 8]. In [8] this asymmetry was found significantly correlated to the diameter at different levels of the ascending aorta, suggesting that the flow deflection plays a crucial role in the ascending aorta dilatation. A second fluid-dynamic phenomenon reported so far consists in the observation that increased haemodynamic viscous forces placed on the proximal aorta could result in a possible progressive aortic dilatation [7]. These two phenomena were linked together by the observation that the flow asymmetry was found to be strictly related to increased and localized wall shear stresses exerted on the dilated lumen surface, as highlighted in [3, 13, 23, 22], and they were observed independently of the dilatation of the ascending aorta.

In recent years, a third fluid-dynamic phenomenon characterizing BAV patients was highlighted, an helical systolic flow in the ascending aorta in presence of BAV [14], accompanied by the presence of a marked systolic retrograde flow [3]. In this paper we tried to elucidate the connections between flow asymmetry and high localized WSS, on one hand, and helical flow and flow reversal, on the others, in BAV patients with a dilated ascending aorta. To this end, we studied the blood flow patterns in such cases by means of both numerical simulations and in-vivo data analysis with the rationale of using the findings from numerical simulations as a key for interpreting in-vivo phenomena. We performed a computational parametric study by varying, for a selected geometry, the valve area and the flow rate entering the aorta and, to perform comparisons, considering also a tricuspid case drawn in the same dilated aorta geometry. Finally we considered in-vivo data obtained by PC-MRI sequences in four BAV and in four TAV cases.

To provide an objective quantification of the phenomena, we introduced a set of indices: the flow reversal ratio (FRR) to measure the presence of retrograde flow, the normalized flow asymmetry (NFA) index [20] to monitor the deviation of the systolic jet, WSSRegion and WSSSlice indices [22] to quantify the systolic WSS and its localization, and the new positive helic fraction (PHF) index

to quantify the degree of uniqueness of the helical flow. Except WSSRegion and WSSSlice which have been considered only for the numerical results, all the indices have been computed both for the numerical results and for the in-vivo imaging data. In [3] the authors measured the FRR on through-plane phase contrast MRI acquired 1-3 cm above the most distal feature of the sinotubular junction in 15 BAV and 15 control patients, demonstrating the reliability of this index in distinguishing between BAV and controls. In [20] the authors demonstrated that NFA index is a more reliable quantitative parameter for measuring systolic jet deviation than flow jet angle, suggesting the use of this parameter to study flow deviation in BAV. WSSRegion and WSSSlice indices were proposed in [22] and have been seen to be highly correlated with the asymmetry of the blood jet. The positive helic fraction has been proposed here with the purpose of having a quantitative synthetic index able to distinguish among single helical flow, double helical flow and absence of helical flow.

Relation between single helical and asymmetric flows. BAV vs TAV. Both numerical and imaged-based results highlighted that BAV patients featured higher values of FRR, NFA and PHF indices when compared with those obtained in TAV configurations (see Tables 3, 4, 7 and 8). Also, high WSS values were found to be strongly localized in BAV cases with respect to TAV, confirming the trend observed in [22] also for a dilated ascending aorta (see Tables 5 and 6). This clearly confirmed that the fluid-dynamics in a dilated ascending aorta in presence of BAV is markedly different from a TAV case featuring the same geometry. Indeed, it is characterized by high flow reversal, high flow asymmetry (see Fig. 6) and the presence of a single right-handed vortex (see Fig. 8 and 9). This is also clearly seen in Fig. 5, where the TAV case (on the right) featured two lateral vortices (one right-handed and one left-handed) which "allows" the blood jet entering the aorta to reach the mid-ascending section by passing through the center of the vessel, leading to a nearly symmetric flow. Viceversa, in the BAV cases (see figures in the left and middle), a single large right-handed vortex is observed, which fills up the central region of the vessel, forcing the blood jet to interplay the mid-ascending aorta by passing close to the aortic wall. This shows that in a dilated ascending aorta with normally functioning BAV, there is a clear correlation among the formation of a single right-handed vortex, the presence of flow reversal and the deflection of the blood jet. This is in strong agreement with what was qualitatively observed through 4D PC-MRI images by Hope [14] who identified the presence of a systolic helical flow associated with eccentric systolic flow jet in 15 of 20 BAV patients but in none of normal or dilated TAV patients. We observe that our results were found for BAV patients without aortic coarctation or tetralogy of Fallot.

Observing the flow pattern in Fig.5 we can hypothesize that the flow asymmetry induces the blood flow to fill up the central region of the vessel, leading to a single vortex. At the same time, it may be speculated that jet deflection toward the wall is exaggerated by the formation of a single vortex, since the flow maybe bumps on the pressure bubble created by the vortex, accentuating its

asymmetry. Therefore the two phenomena seem to be strongly interconnected and markedly related to BAV orifice morphology as evidenced by the results obtained when varying the valve area.

Relation between single helical and asymmetric flows. Varying flow rate and valve orifice area for BAV. By analyzing Tables 3, 4, 7 and 8, we observed that indices FRR, NFA and PHF featured a similar behavior both for the numerical results and for the in-vivo data. In particular, they both increased by decreasing the valve orifice area and/or by increasing the value of the flow rate. This further confirmed the strong connection between the formation of a single right-handed helical flow and blood jet deflection. Again, this is confirmed by observing Fig. 5, left, where a large valve orifice area and a small flow rate lead to a single vortex and asymmetry, that are less pronounced than in the case reported on the middle, featuring a smaller valve area and a larger flow rate.

By analyzing the values of indices NFA and PHF both for numerical and for in-vivo results, we can characterize the two groups featuring high values (Bn1 and Bn2-F4 for numerical results, and B1, B2 and B3 for in-vivo results), by introducing the group characterized by the following values:
- valve/root area ratio $A_{val}/A_{root} = 0.29$ with systolic flow rate $F > 18\,l/min$, or
- valve/root area ratio $A_{val}/A_{root} < 0.29$.
This group is characterized by values $NFA > 0.45$ and $PHF > 0.8$. Similarly, the BAV groups featuring intermediate values of NFA and PHF (Bn2-F2, Bn2-F3 and Bn3 for the numerical results, and B4 for the in-vivo results) could be characterized by the following values:
- valve/root area ratio $A_{val}/A_{root} = 0.29$ with systolic flow rate $F < 18\,l/min$, or
- valve/root area ratio $A_{val}/A_{root} > 0.29$.
This group is characterized by values $0.2 < NFA < 0.4$ and $0.5 < PHF < 0.7$. The only case which did not obey this trend is BAV patient B2 which featured $PHF = 0.55$. This could be explained by the fact that for this case $F = 7.9\,l/min$, a value which is considerably less than those used in the numerical simulations and featured by the two other patients of the first group.

Clinical implications. As observed, high and localized WSS in the ascending aorta are the effect of the blood jet deflection. For this reason, in [22] we proposed to use flow asymmetry (easily evaluated by imaging) as a surrogate of the localization of high WSS in the ascending aorta, and then as a simple indicator of the possible risk of dilatation. In addition, due to the relation between flow asymmetry and presence of a single vortex, we propose the presence of a single vortex in a dilated ascending aorta as a surrogate marker of high localized WSS in the ascending aorta.

Agreement between numerical and in-vivo data. The results presented in this work showed an excellent agreement between the numerical simulations and the in-vivo analyses obtained by means of PC-MRI sequences. This is an important point for future analyses, since it highlights the reliability of computational tools

for such investigations.

Limitations. Limitations of our study rely on the availability of few in-vivo data. A more comprehensive study is mandatory to better understand our first highlighted results. The main model limitation of this work concerns some of the hypotheses introduced for the numerical simulations. In particular, the assumption of rigid walls is probably simplistic, since the motion of the aorta (due both to the interaction with blood and to the rigid movement of the heart) is not negligible. However, we argued that, owning to the good agreement between imaging and simulation data, the modeling strategy we adopted is adequate for the scope of the present work.

Moreover, we did not take into account the valve opening and closing mechanisms, in fact all our numerical simulations were performed with an open valve configuration without the presence of the leaflets. This is a very interesting point, since our results highlighted that the flow asymmetry is already generated (with values of NFA comparable to those extracted by in-vivo data) *without* modeling the leaflets. This infers that probably the particular shape of the orifice in BAV cases (not necessarily, or in addition to, the presence of the leaflets, as suggested in [6]) is the primary cause in the generation of the flow deflection.

5   Acknowledgments

References

[1] Antiga, L., M. Piccinelli, L. Botti, B. Ene-Iordache, A. Remuzzi, and D. A. Steinman. An image-based modeling framework for patient-specific computational hemodynamics. Med. Biol. Eng. Comput. 46:1097-1112, 2008.

[2] Baltes, C., M. S. Hansen, J. Tsao, S. Kozerke, R. Rezavi, E. M. Pedersen, and P. Boesiger. Determination of peak velocity in stenotic areas: echocardiography versus k-t SENSE accelerated MR Fourier velocity encoding. Radiology 246:249-257, 2008.

[3] Barker, A. J., C. Lanning, and R. Shandas. Quantification of hemodynamic wall shear stress in patients with bicuspid aortic valve using Phase-Contrast MRI. Ann. Biomed. Eng. 38:788-800, 2010.

[4] Barker, A. J. and M. Markl. The role of hemodynamics in bicuspid aortic valve disease. Eur. J. Cardio-Thoracic Surgery 39:805-806, 2011.

[5] Bauer, M., V. Gliech, H. Siniawski, and R. Hetzer. Configuration of the ascending aorta in patients with bicuspid and tricuspid aortic valve disease

undergoing aortic valve replacement with or without reduction aortoplasty. J. Heart Valve Dis. 15:594-600, 2006.

[6] Della Corte, A., C. Bancone, C. A. Conti, E. Votta, A. Redaelli, L. Del Viscovo, and M. Cotrufo. Restricted cusp motion in right-left type of bicuspid aortic valves: a new risk marker for aortopathy. J. Thorac. Cardiovasc. Surg. , 2011.

[7] Della Corte, A., C. Quarto, C. Bancone, C. Castaldo, F. Di Meglio, D. Nurzynska, L. S. De Santo, M. De Feo, M. Scardone, S. Montagnani, and M. Cotrufo. Spatiotemporal patterns of smooth muscle cell changes in ascending aortic dilatation with bicuspid and tricuspid aortic valve stenosis: Focus on cell-matrix signaling. J. Thorac. Cardiovasc. Surg. 135:8-U44, 2008.

[8] den Reijer, P. M., D. Sallee III, P. van der Velden, E. R. Zaaijer, W. J. Parks, S. Ramamurthy, T. Q. Robbie, G. Donati, C. Lamphier, R. P. Beekman, and M. E. Brummer. Hemodynamic predictors of aortic dilatation in bicuspid aortic valve by velocity-encoded cardiovascular magnetic resonance. J. Cardiovasc. Magn. Reson. 12:4, 2010.

[9] Formaggia, L., A. Quarteroni, and A. Veneziani. Cardiovascular Mathematics: Modeling and simulation of the circulatory system. : Springer Verlag, 2009.

[10] Girdauskas, E., M. A. Borger, M. Secknus, G. Girdauskas, and T. Kuntze. Is aortopathy in bicuspid aortic valve disease a congenital defect or a result of abnormal hemodynamics? A critical reappraisal of a one-sided argument. Eur. J. Cardio-Thoracic Surgery 39:809-814, 2011.

[11] Hahn, R. T., M. J. Roman, A. H. Mogtader, and R. B. Devereux. Association of aortic dilation with regurgitant, stenotic and functionally normal bicuspid aortic valves. J. Am. Coll. Cardiol. 19:283-288, 1992.

[12] Haycock, G. B., G. J. Schwartz, and D. H. Wisotsky. Geometric method for measuring body surface area: a height-weight formula validated in infants, children, and adults. J. Pediatr. 93:62-66, 1978.

[13] Hope, M. D., T. A. Hope, S. E. S. Crook, K. G. Ordovas, T. H. Urbania, M. T. Alley, and C. B. Higgins. 4D Flow CMR in assessment of valve-related ascending aortic disease. Jacc-Cardiovascular Imaging 4:781-787, 2011.

[14] Hope, M. D., T. A. Hope, A. K. Meadows, K. G. Ordovas, T. H. Urbania, M. T. Alley, and C. B. Higgins. Bicuspid aortic valve: four-dimensional MR evaluation of ascending aortic systolic flow patterns. Radiology 255:53-61, 2010.

[15] Hope, T. A., M. Markl, L. Wigstrom, M. T. Alley, D. C. Miller, and R. J. Herfkens. Comparison of flow patterns in ascending aortic aneurysms and volunteers using four-dimensional magnetic resonance velocity mapping. J. Magn. Resonance 26:1471-1479, 2007.

[16] Keane, M. G., S. E. Wiegers, T. Plappert, A. Pochettino, J. E. Bavaria, and M. G. S. Sutton. Bicuspid aortic valves are associated with aortic dilatation out of proportion to coexistent valvular lesions. Circulation 102:35-39, 2000.

[17] Nichols, W. and M. O'Rourke. McDonald's Blood Flow in Arteries: Theoretical, Experimental, and Clinical Principles. 1998. London: Edward Arnold .

[18] Nkomo, V. T., M. Enriquez-Sarano, N. M. Ammash, L. J. Melton, K. R. Bailey, V. Desjardins, R. A. Horn, and A. J. Tajik. Bicuspid Aortic Valve Associated With Aortic Dilatation A Community-Based Study. Arterioscler. Thromb. Vasc. Biol. 23:351-356, 2003.

[19] Roman, M. J., R. B. Devereux, R. Kramer-Fox, and J. O'Loughlin. Two-Dimensional Echocardiographic Aortic Root Dimensions in Normal Children and Adults. Am. J. Cardiol. 64:507-512, 1989.

[20] Sigovan, M., M. D. Hope, P. Dyverfeldt, and D. Saloner. Comparison of Four-Dimensional Flow Parameters for Quantification of Flow Eccentricity in the Ascending Aorta. J. Magn. Resonance 34:1226-1230, 2011.

[21] Veneziani, A. and C. Vergara. Flow rate defective boundary conditions in haemodynamics simulations. Int. J. Numer. Methods Fluids 47:803-816, 2005.

[22] Vergara, C., F. Viscardi, L. Antiga, and G. B. Luciani. Influence of bicuspid valve geometry on ascending aortic fluid dynamics: a parametric study. Artif. Organs 36:368-378, 2012.

[23] Viscardi, F., C. Vergara, L. Antiga, S. Merelli, A. Veneziani, G. Puppini, G. Faggian, A. Mazzucco, and G. B. Luciani. Comparative Finite Element Model Analysis of Ascending Aortic Flow in Bicuspid and Tricuspid Aortic Valve. Artif. Organs 34:1114-1120, 2010.

MOX Technical Reports, last issues

Dipartimento di Matematica "F. Brioschi",
Politecnico di Milano, Via Bonardi 9 - 20133 Milano (Italy)

19/2012 FAGGIANO, E.; ANTIGA, L.; PUPPINI, G.; QUARTERONI, A.; LUCIANI G.B.; VERGARA, C.
Helical Flows and Asymmetry of Blood Jet in Dilated Ascending Aorta with Normally Functioning Bicuspid Valve

18/2012 FORMAGGIA, L,; VERGARA, C.
Prescription of general defective boundary conditions in fluid-dynamics

17/2012 MANZONI, A.; QUARTERONI, A.; GIANLUIGI ROZZA, G.
Computational reduction for parametrized PDEs: strategies and applications

16/2012 CUTRI', E.; ZUNINO, P.; MORLACCHI, S.; CHIASTRA, C.; MIGLIAVACCA, F.
Drug delivery patterns for different stenting techniques in coronary bifurcations: a comparative computational study

15/2012 MENGALDO, G.; TRICERRI, P.; CROSETTO,P.; DEPARIS, S.; NOBILE, F.; FORMAGGIA, L.
A comparative study of different nonlinear hyperelastic isotropic arterial wall models in patient-specific vascular flow simulations in the aortic arch

14/2012 FUMAGALLI, A.;SCOTTI, A.
An unfitted method for two-phase flow in fractured porous media.

13/2012 FORMAGGIA, L.; GUADAGNINI, A.; IMPERIALI, I.; LEVER, V.; PORTA, G.; RIVA, M.; SCOTTI, A.; TAMELLINI, L.
Global Sensitivity Analysis through Polynomial Chaos Expansion of a basin-scale geochemical compaction model

12/2012 GUGLIELMI, A.; IEVA, F.; PAGANONI, A.M.; RUGGERI, F.
Hospital clustering in the treatment of acute myocardial infarction patients via a Bayesian semiparametric approach

11/2012 BONNEMAIN, J.; FAGGIANO, E.; QUARTERONI A.; DEPARIS S.
A Patient-Specific Framework for the Analysis of the Haemodynamics in Patients with Ventricular Assist Device

10/2012   Lassila, T.; Manzoni, A.; Quarteroni, A.; Rozza, G.
Boundary control and shape optimization for the robust design of bypass anastomoses under uncertainty